# Surface Structure of Zeolite (MFI) Crystals

**ARTICLE** *in* CHEMISTRY OF MATERIALS · DECEMBER 2004

Impact Factor: 8.35 · DOI: 10.1021/cm0488534



**4 AUTHORS**, INCLUDING:

Osamu Terasaki
Stockholm University
**454** PUBLICATIONS **21,489** CITATIONS
SEE PROFILE

Michael Tsapatsis
University of Minnesota Twin Cities
**291** PUBLICATIONS **9,098** CITATIONS
SEE PROFILE

# *Articles*

## Surface Structure of Zeolite (MFI) Crystals

Isabel Díaz,[†,§] Efrosini Kokkoli,[†] Osamu Terasaki,[‡] and Michael Tsapatsis*[,†]

*Department of Chemical Engineering and Materials Science, University of Minnesota, Minneapolis, Minnesota 55455, Arrhenius Laboratory, Stockholm University, S-106 91 Stockholm, Sweden*

*Received July 14, 2004. Revised Manuscript Received September 13, 2004*

Silicalite-1 (structure type MFI) is an important zeolite that, in addition to conventional applications such as adsorption and catalysis and emerging applications such as thin films and membranes, is often used as a model system in studies of zeolite crystal growth. The surface structure of silicalite-1 crystals with two different morphologies (hexagonal prismatic and leaf-shaped platelike crystals), synthesized in the presence of two different structure-directing agents (SDAs) (tetrapropylammonium (TPA) cation and the trimer of TPA, respectively), is elucidated by high-resolution transmission electron microscopy and atomic force microscopy. The differences and similarities in crystal shape and external surface termination are interpreted based on SDA fitting in the crystal structure and adsorption kinetics of the SDAs on the external surfaces of the growing crystals.

### Introduction

Silicalite-1 (structure type MFI)[1] is an important siliceous zeolite that, in addition to industrial use, is considered as a promising membrane material[2,3] and is often used as a model system in studies attempting to elucidate aspects of the mechanism of hydrothermal crystal growth.[4−11]

Information on the external surface structure of zeolite crystals is needed in order to build reliable mathematical models of zeolite crystal growth[5] and evaluate different possible crystal growth mechanisms.[6] It may also be useful in understanding catalytic and adsorption properties, especially when crystal sizes approach nanoscale dimensions and the role of external surface becomes of increased significance.

High-resolution transmission electron microscopy (HRTEM) can be used to elucidate the external surface structure of zeolites.[12−14] However, no such studies can be found up to now for MFI, and we know only of atomic force microscopy (AFM) studies on the surface structure of MFI.[6] Here, we examine by HRTEM and AFM the external surface of silicalite-1 crystals synthesized in the presence of two struture-directing agents (SDAs), the tetrapropylammonium cation (TPA) and the trimer TPA cation, bis-*N*,*N*-(tripropylammoniumhexamethylene)di-*N*,*N*-propylammonium trihydroxide, hereafter noted as tC6.

The MFI structure is described as a combination of two interconnected channel systems. The silicate framework forms sinusoidal 10-member-rings (MR) channels along the direction of the *a*-axis, interconnected with 10-MR straight channels that run down the *b*-axis. A tortuous pore path is present along the *c*-axis. The MFI framework model can be build by connecting pentasil silicate chains. Figure 1 shows a schematic of the channel system along with the framework projections and the structure of the pentasil chain. The characteristic crystal shape of TPA-silicalite-1 is a hexagonal prismatic shape, also referred to as a coffin shape, with the order of crystal dimensions L*c* > L*a* > L*b* (where L*i*

* Corresponding author. E-mail: tsapatsi@cems.umn.edu. Tel: +1-612-626-0920. Fax: +1-612-626-7246.
† University of Minnesota.
‡ Stockholm University.
§ Currently at the Instituto de Catálisis y Petroleoquímica, CSIC, Campus Cantoblanco, 28049 Madrid, Spain.

(1) Database of the Structure Commission of the International Zeolite Association (www.iza-structure.org/databases).
(2) Yuan, W. H.; Lin, Y. S.; Yang, W. S. *J. Am. Chem. Soc.* **2004**, *126* (15), 4776−4777.
(3) Lai, Z. P.; Bonilla, G.; Diaz, I.; Nery, J. G.; Sujaoti, K.; Amat, M. A.; Kokkoli, E.; Terasaki, O.; Thompson, R. W.; Tsapatsis, M.; Vlachos, D. G. *Science* **2003**, *300* (5618), 456−460.
(4) Schoeman, B. J. *Microporous Mesoporous Mater.* **1998**, *22*, 9−22.
(5) Nikolakis, V.; Tsapatsis, M.; Vlachos, D. G. *Langmuir* **2003**, *19* (11), 4619−4626.
(6) Agger, J. R.; Hanif, N.; Cundy, C. S.; Wade, A. P.; Dennison, S.; Rawlinson, P. A.; Anderson, M. W. *J. Am. Chem. Soc.* **2003**, *125* (3), 830−839.
(7) Burkett, S. L.; Davis, M. E. *Chem. Mater.* **1995**, *7* (5), 920−928. Burkett, S. L.; Davis, M. E. *Chem. Mater.* **1995**, *7* (8), 1453−1463.
(8) Navrotsky, A.; Petrovic, I.; Hu, Y.; Chen, C. Y.; Davis, M. E. *J. Non-Cryst. Solids* **1995**, *193*, 474−477.
(9) de Moor, P.; Beelen, T. P. M.; van Santen, R. A.; Beck, L. W.; Davis, M. E. *J. Phys. Chem. B* **2000**, *104* (32), 7600−7611.
(10) Serrano, D. P., van Grieken, R. *J. Mater. Chem.* **2001**, *11*, 2391−2407.
(11) Corma, A.; Davis, M. E. *ChemPhysChem* **2004**, *5* (3), 304−313.
(12) Ohsuna, T.; Horikawa, Y.; Hiraga, K.; Terasaki, O. *Chem. Mater.* **1998**, *10* (3), 688−691.
(13) Alfredsson, V.; Ohsuna, T.; Terasaki, O.; Bovin, J.-O. *Angew. Chem. Int. Ed.* **1993**, *32* (8), 1210−1213.
(14) Slater, B.; Catlow, C. R. A.; Liu, Z.; Ohsuna, T.; Terasaki, O.; Camblor, M. A. *Angew. Chem. Int. Ed.* **2002**, *41* (7), 1235−1237.

10.1021/cm0488534 CCC: $27.50 
Published on Web 11/10/2004

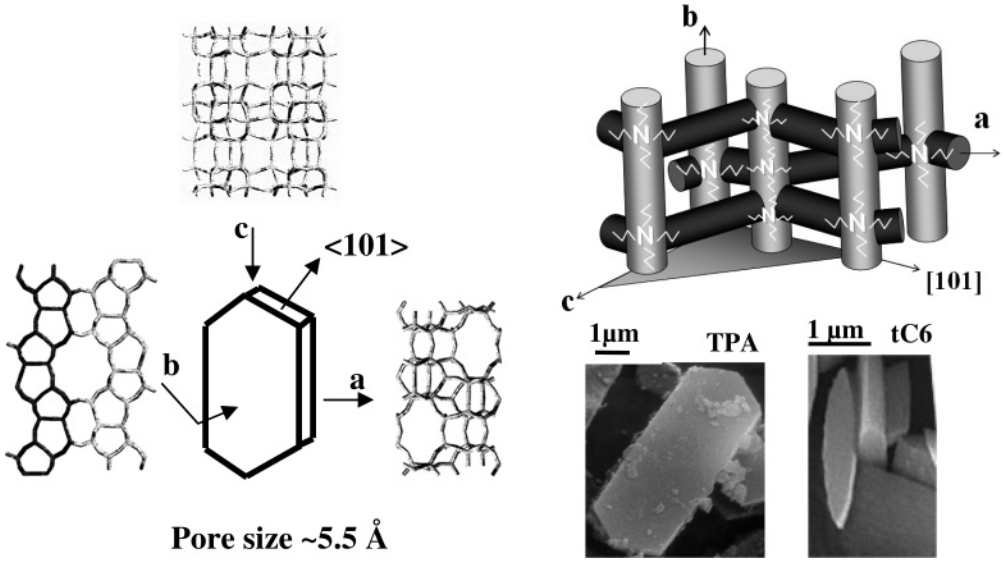


**Figure 1.** Schematic of the pore structure of TPA-MFI with the TPA located at channel intersections (top right). Typical SEM images of coffin-shaped crystals grown with TPA and leaf-shaped platelike crystals grown with tC6 are shown at the bottom right. A schematic identifying the crystal faces and dimensions along with the corresponding framework projections is given in the left part of the figure. The pentasil chain is highlighted.

indicates crystal size along *i*-axis). The MFI crystal shape can be modified by use of different SDAs.[15,16] Use of tC6 as SDA[17] leads to platelike leaf-shaped crystals with L$c$ > L$b$ > L$a$.[3,16] The two characteristic crystal shapes grown by TPA and tC6 are included in Figure 1 along with the crystal structure schematics of the MFI framework.

## Experimental Section

Synthesis of the templates and the corresponding zeolites have been reported separately elsewhere.[16] Crystal morphology and size were determined using scanning electron microscopy (SEM). The samples were dispersed onto carbon tape and coated with a gold/palladium alloy using a Polaron E5100 sputter coater system. The zeolite crystals were then observed on a JEOL JSM-5400 microscope operating in SEM mode at 15 kV. Transmission electron microscopy (TEM) coupled with selected area electron diffraction (SAED) was used to index the crystal faces and study the surface structure. HRTEM images and SAED patterns were taken with a JEOL ARM 1250 microscope operating at 1250 kV (Cs = 1.7 mm). For the observations, the samples were dispersed in acetone and placed on a holey carbon microgrid for analysis. AFM characterization of *b*-oriented films was done with a Digital Instruments Nanoscope III system (Digital Instruments, Santa Barbara, CA). Images were obtained in contact mode in air using standard 200-mm V-shaped oxide-sharpened silicon nitride AFM cantilevers with pyramidal tips (Digital Instruments) of nominal radius 5−40 nm and nominal spring constant 0.06 N/m.

## Results and Discussion

Transmission electron microscopy (TEM) images coupled with selected area electron diffraction (SAED) patterns were used to identify the corresponding crystal faces. The smaller zeolite crystals obtained from the seeded synthesis using TPA and tC6 were calcined prior to the TEM/SAED analysis. By tilting the crystals it was possible to align the tC6 grown crystals with the electron beam parallel to their *a*-, *b*-, and *c*-axis, i.e., sinusoidal channels, straight channels, and tortuous paths parallel to the electron beam, respectively. Figure 2 shows low-magnification TEM images and the corresponding SAED patterns of the [100], [010], and [001] (from the top to bottom of the image) projections of tC6 grown crystals. In this figure, scanning electron micrographs (SEM), marked with white arrows, are shown as well for better understanding of the crystal projections. The TEM observation shows that the elongated oval shape projection of the crystals synthesized using tC6 corresponds to a view down the direction of the straight channels, [010]. The rectangular projection viewed down the thinner dimension of the crystals corresponds to the [100] direction, along which run the sinusoidal channels.

As a starting point, the change in crystal morphology by use of tC6 in place of TPA as SDA can be explained following the arguments of de Vos Burchart et al.[15,16] According to these arguments, the relative crystal size along the *a*- and *b*-axis can be interpreted in terms of how well the SDA fits in the straight (*b*-axis) versus the sinusoidal (*a*-axis) channels. Molecular mechanics simulations suggested that the dimers of TPA will be located with their long dimension almost exclusively extending along the *b*-axis. While simulations are not available for the tC6, its preference for the straight channel versus the sinusoidal channel should be more pronounced than that of the dimer.[16]

To further understand MFI crystal morphology modification by different SDAs information beyond the fitting of the SDA in the framework, like the structure of growth units and their rate of attachment on the zeolite surface, is desirable. Regarding the structure of growth units, it has been established that subcolloidal particles of size and shape similar to the ones observed during growth with TPA are present during nucleation and growth with dC6 and tC6.[9] However, the role of these particles and their degree of participation in growth is

(15) de Vos Burchart, E.; Jansen, J. C.; van de Graaf, B.; van Bekkum, H. *Zeolites* **1993**, *13*, 216−221.
(16) Bonilla, G.; Díaz, I.; Tsapatsis, M.; Jeong, H.-K.; Lee, Y.; Vlachos, D. G. *Chem. Mater.* submitted.
(17) Beck, L. W.; Davis, M. E. *Microporous Mesoporous Mater.* **1998**, *22* (1−3), 107−114.

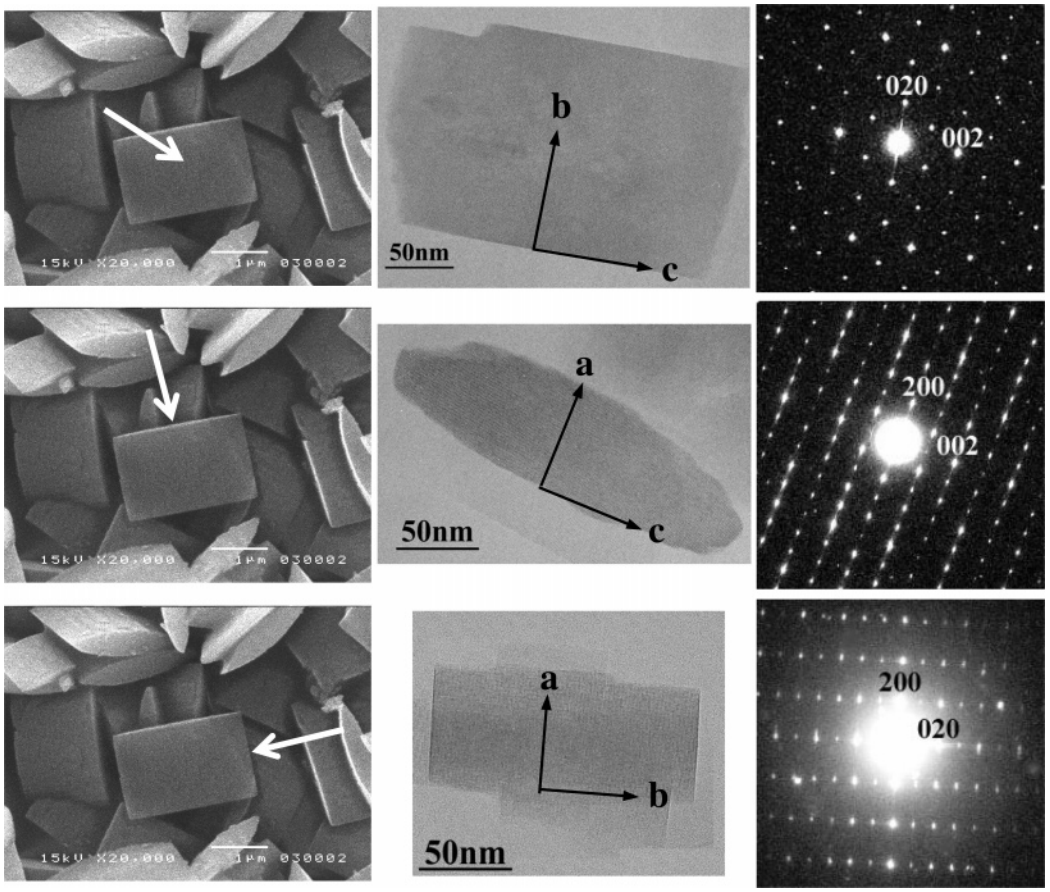


**Figure 2.** SEM, low-magnification TEM images, and SAED patterns of silicalite-1 *b*-elongated leaf-shaped crystals grown with tC6. The zone axes are [100] (top), [010] (middle), and [001] (bottom).

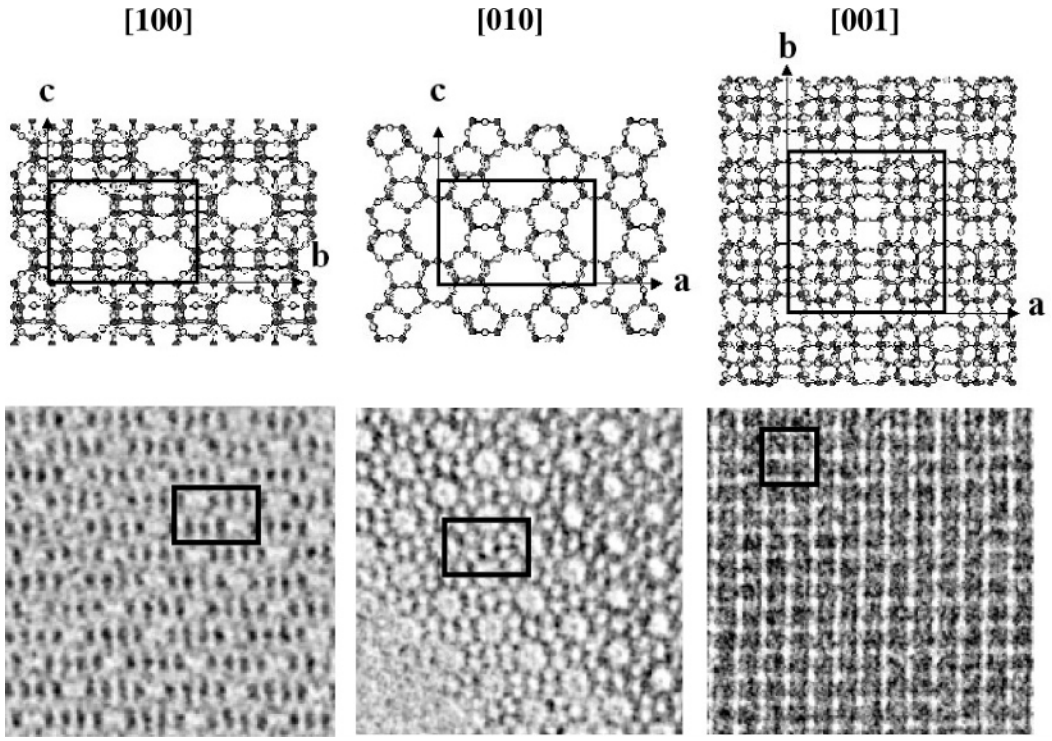


**Figure 3.** Schematics of crystallographic projections along *a*-, *b*-, and *c*-axis (top from left to right) and corresponding HRTEM images (bottom).

not yet clear. It is possible that attachment followed by rearrangements or even oriented attachment prevail. If growth by addition of subcolloidal particles dominates, SDA adsorption and desorption along with subcolloidal particle attachment and rearrangement determine the growth rate of the different faces.[5] At the other extreme, it is possible that the subcolloidal particles are spectator species and serve as a pool of nutrients by slow release

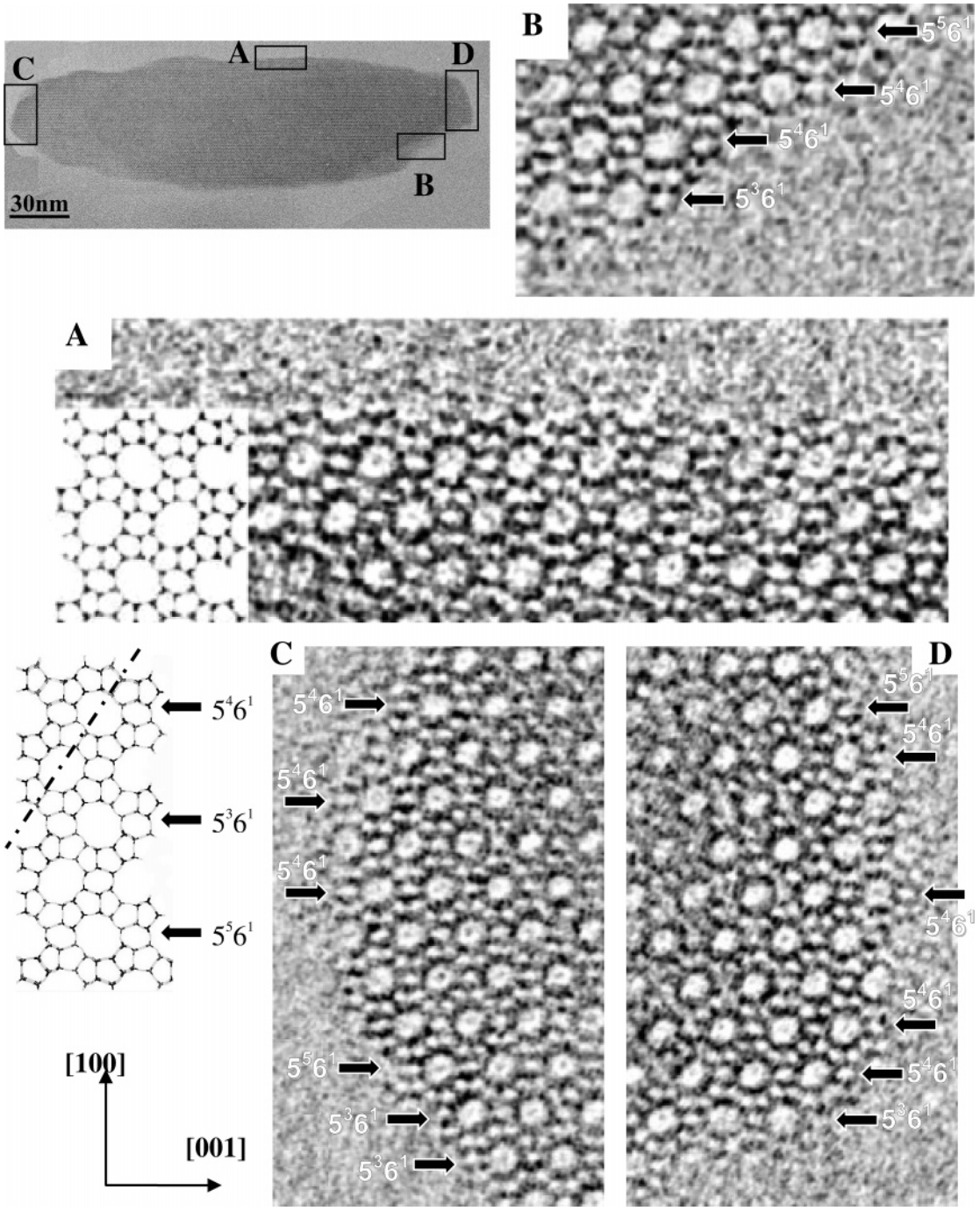


**Figure 4.** Low-magnification HRTEM image of tC6-grown crystal viewed down the *b*-axis (straight channels). Higher magnifications: area A shows termination of the (100) face with complete pentasil chains and sections of incomplete 6MRs. Various (*h*0*l*) terminations are shown in B, C, and D. The arrows point to the 6MR and the corresponding symbols indicate the number of 5MRs that surround the 6MR. Analysis of several similar images indicates that the predominant termination is a 6MR surrounded by four 5MRs (noted by $5^4 6^1$). A considerable fraction of a 6MR surrounded by three 5MRs ($5^3 6^1$) along with some rougher or hairy terminations with an extra 5MR ($5^5 6^1$) are observed.

of monomeric and oligomeric silicate species during growth. In the case of growth by addition of dissolved silicate species around adsorbed SDA cations, SDA adsorption and desorption and surface nucleation of silicalite layers determine the relative growth rates of the different faces. In any case, information on surface structure of the different crystal faces is necessary for rate estimation of these processes.

In what follows we present our findings on the external surface structure of MFI grown by TPA and tC6. Although HRTEM has been used to study external surface structure of zeolites[12−14] we know of AFM studies only on the surface structure of TPA-grown MFI.[6] Figure 3 shows HRTEM views down the three principal axes of the MFI framework with corresponding schematics of the framework and serves as a reference for identifying surface terminations from the projections down the *a*- and *b*-axis.

**[010]-Projection.** Figure 4 shows the [010] projection of a tC6-grown MFI crystal. The termination of area A provides information on the structure of the (100) face. It indicates termination with complete pentasil chains

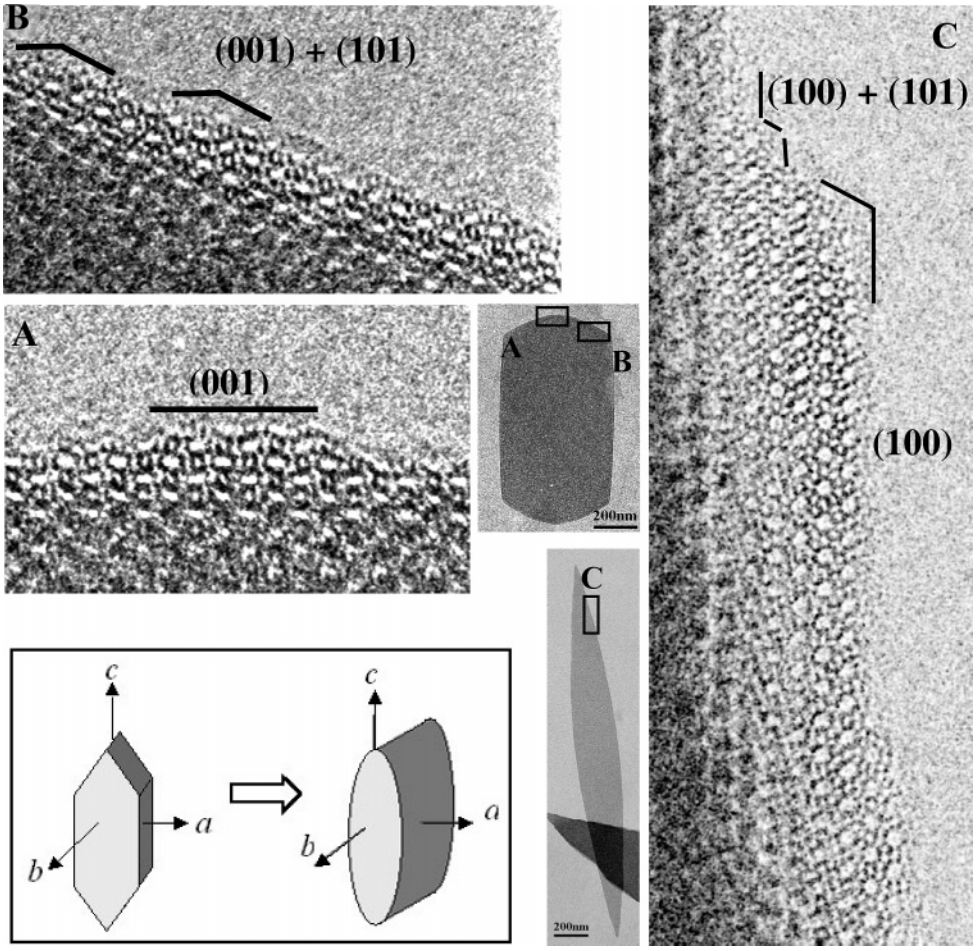


**Figure 5.** Coffin vs leaf-like projections down the *b*-axis. Insets A and B show the combination of (001) and (101) facets giving rise to the curved upper face of the TPA-MFI crystal. The (001) face can be described as a combination of neighboring (101) and ($\bar{1}$01) facets. The absence of such combinations leads to the leaf-like crystals grown by dC6 and tC6 as shown in inset C.

and incomplete six-member rings (6MR). Areas B, C, and D indicate the absence of other well-defined facets in this projection. The (*h*0*l*) facets are formed by various combinations of a terminal 6MR with 5MRs. Although groups consisting of a 6MR surrounded by four 5MRs (indicated by $5^4 6^1$) are most abundant (in excess of 50%), a considerable fraction of a 6MR surrounded by three 5MRs ($5^3 6^1$) along with some rougher or hairy terminations with an extra 5MR ($5^5 6^1$) are observed. Examination of TPA-grown crystals (Figure 5) yields similar surface terminations with only one significant difference, the presence of (001) faces which consist of sequential (101) + ($\bar{1}$01) terminations. Such facets are absent in the tC6 grown crystals. Although an explanation for this difference is beyond the scope of this work, this additional termination can phenomenologically account for the differences between the [010] projection of the coffin-shape vs leaf-like crystals.

**[100]-Projection.** Figure 6 shows a view down the sinusoidal channels of a tC6-grown crystal. The area marked A provides information on the surface termination of the (010) faces. Magnification of the mentioned area shows the presence of ~1-nm steps ($^1/_2$ unit cell along the *b*-axis), while magnification B shows a rare ~2-nm step (one unit cell along the *b*-axis). The bottom image shows an enlargement of Figure 6A. The sequence of 2, 4, 2, 4 black dots as indicated in this image clearly establishes as dominant termination of the (010) face complete pentasil chains and incomplete 6MRs. This surface structure minimizes the number of Si−OH groups and has been often proposed as a possible surface termination.

We have not been able to acquire HRTEM images of TPA-MFI crystals down the *a*-axis. However, we performed AFM imaging of such surfaces using *b*-oriented MFI films and we found step heights of ~1 nm in agreement with the results reported in ref 6. In examining TPA-MFI crystals by AFM, we have observed surfaces with terraces similar to those of ref 6. Also, for smaller TPA-MFI crystals, (010) surfaces with rectangular islands are common. A typical AFM image of the (010) face of such a TPA-MFI crystal is shown in Figure 7. It shows 10 × 10 nm islands with height ~1±0.3 nm. Although we observe islands instead of the concentric terraces, the step height determined here is similar to that of ref 6 indicating that the dominant surface termination is not affected by the growth mode. It appears, therefore, that step heights and most likely surface termination for the (010) faces of TPA and tC6 grown crystals are the same. For the tC6 grown crystals, at least two other rare (010) surface terminations have been identified and they will be reported in a future correspondence.

**A Possible Growth Mechanism Along *a*- and *b*-Axis: Multiple- vs One-Site SDA Adsorption.** Given the similarity of the external surface of MFI crystals grown by TPA and tC6 established by this study and ref 6 and the reported similarity of subcolloidal

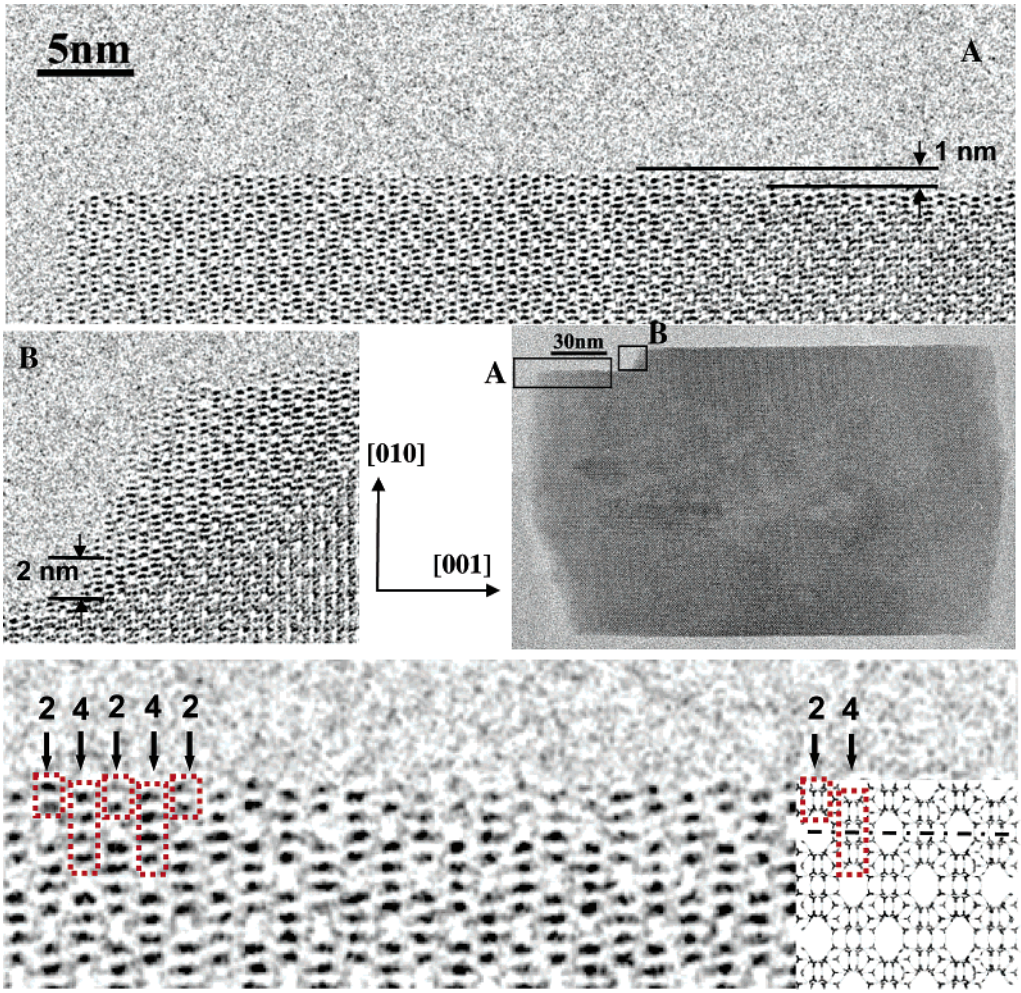


**Figure 6.** HRTEM image of tC6-grown crystals down the *a*-axis (sinusoidal channels). Predominant 1-nm steps along [010] are indicated at high magnification in A. A more rare 2-nm step along [010] is shown in B. An enlarged HRTEM image down [100] (lower part of the figure) shows the surface termination of the (010) face. The rectangular inserts in the image indicate the 2, 4, 2, 4 contrast mentioned in the text, and help identify the termination by a complete pentasil chain (see also insert with crystal structure scheme).

entities in the two systems,[9] it is worth addressing in some detail a possible mechanism capable of explaining the observed differences of the relative growth rates along the different directions especially along the *a*- and *b*-axis. Agger et al. argued that the different growth rates along *b*- and *a*-axis of TPA-grown MFI can be attributed to differences in surface nucleation rates rather than step propagation rates.[6] A 4-fold difference between nucleation of a pentasil layer on the (100) vs (010) surface was proposed for the particular well-developed crystals examined. To follow a similar argument for the well-developed (010) face of tC6-grown MFI we add that nucleation of the next layer relies first on adsorption of the tC6 end-on with one of its propyl groups pointing inside the straight channel. This can be considered as a one-site adsorption, with the site being the MFI pore mouth. This step does not appear to be rate-limiting based on the following argument. Adsorption of a single tC6 layer on the (010) face extending along the *b*-axis can direct the growth of three pentasil layers as opposed to two pentasil layers for dC6 and one pentasil layer for a layer of TPA. Given that the dominant step on the (010) face for tC6-grown crystals is ~1 nm, i.e., a single pentasil layer (similar to that of TPA-grown crystals), it can be concluded that pentasil layer formation rather tC6 adsorption is rate limiting. It follows that formation of the next two pentasil layers will not require tC6 adsorption and, consequently, the use of tC6 instead of TPA will not have a positive or adverse effect on nucleation and growth of pentasil layers on the (010) face. The situation on the (100) face will be drastically different. Nucleation of a pentasil layer requires adsorption of tC6 appropriately aligned with its long dimension along the *b*-direction with three propyl chains (one for each consecutive nitrogen atom) pointing inside the openings of three nearest neighboring sinusoidal channels. This can be described as a three site adsorption and therefore, more kinetically hindered. The presence of rough and not well developed (*h*0*l*) faces for tC6 grown crystals suggests that nucleation of a pentasil layer, although undoubtedly more difficult compared to that on a (010) face, is not rate limiting. Instead, terrace or island spreading appears to be considerably hindered by the stringent requirement of three site aligned adsorption of tC6. The mechanism described above points to an inhibiting role of tC6 when adsorbed in the more probable but wrong orientations on the (*h*0*l*) faces. This scenario appears adequate to account for the trends observed regarding relative growth rates along the *a*-

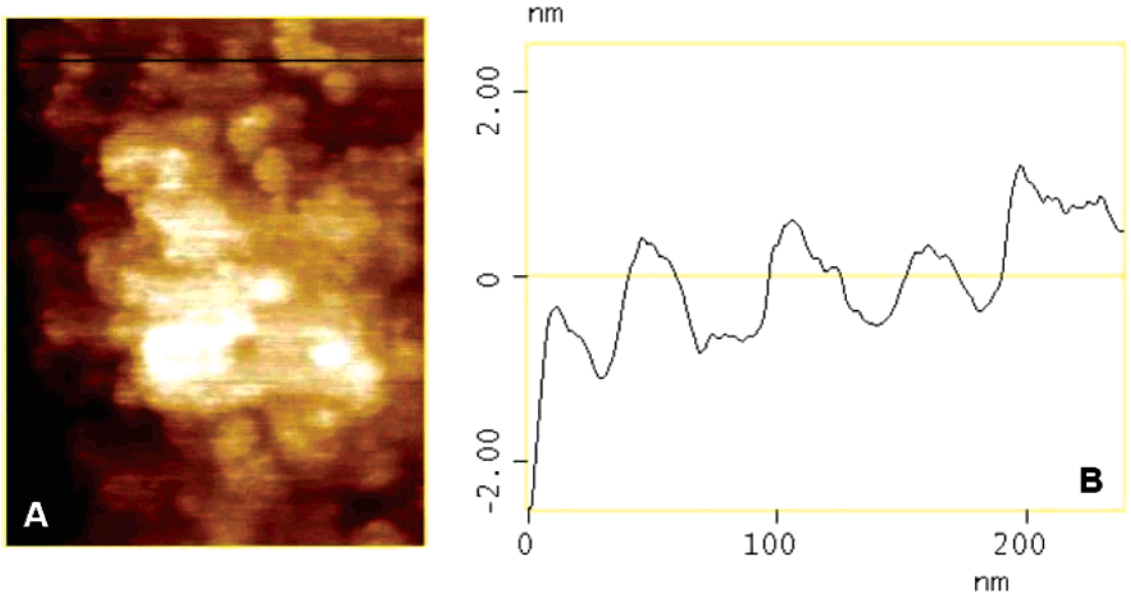


**Figure 7.** (A) AFM image of the (010) surface of TPA-grown silicalite-1. The image is 370 × 250 nm and the height variations in the image are 5 nm. (B) Height variation along the black line indicated in A. The measured heights are 1 ± 0.25 nm.

and *b*-axis for the dC6 and tC6 in comparison to crystals grown by TPA. Of course, it precludes the rate-limiting step for growth on all faces of these well-developed crystals, being the addition of subcolloidal particles as it has been proposed for the growth of TPA-MFI crystals under certain conditions. An attempt to investigate alternative scenarios will be the subject of future work.

## Conclusions

The external surface of TPA-MFI and tC6-MFI crystals is imaged for the first time by HRTEM. Along with previous AFM studies of TPA-MFI crystals, the images indicate similar predominant termination and step heights in the two systems. The presence of (001) faces in TPA-MFI and their absence in tC6-MFI appears to be the main difference. Otherwise *a*- and *b*-faces terminate with complete pentasil chains and incomplete 6MRs minimizing the number of silanol groups, while , the (*h*0*l*) faces terminate with a predominant $5^4 6^1$ unit with a smaller fraction of $5^3 6^1$ and more rare $5^5 6^1$ units.

**Acknowledgment.** We acknowledge G. Bonilla for providing the zeolite samples used for TEM imaging, and Z. Lai for providing the zeolite films used for the AFM imaging. I.D. acknowledges funding from a MECD/Fulbright Postdoctoral Fellowship. Funding for this work was provided by NSF/NIRT (CTS-0103010).

CM0488534